Analysis of distance measurement errors in CW FM sonar with MLS code modulation

Andrzej JEDEL, Jacek MARSZAL, Roman SALAMON

Gdansk University of Technology
Faculty of Electronics, Telecommunications and Informatics
G. Narutowicza 11/12, 80-233 Gdansk, Poland
andrzej.jedel@eti.pg.edu.pl

Although used in the classic silent sonar, the CW FM sounding signal has a major flaw which is its inaccuracy in determining the distance to a target. The authors of the article have developed a concept of silent sonar using frequency modulation signals switched by pseudo-random codes, already discussed in their previous work. This article presents a detailed analysis of errors in CW FM sonar with pseudo-random sequence code modulation confronted with errors which occur in similar sonar without code modulation.

Keywords: CW FM sonar, pseudorandom sequence, Doppler effect, sonar parameters.

1. Introduction

Continuous wave (CW) and linear frequency modulation (FM) sonars have two major advantages over pulse sonars. First, their ability to significantly reduce the acoustic power they emit hampers detection by intercept sonars [5, 6, 9, 10]. Second, they ensure an almost continuous observation of moving targets, a key feature for long-range sonars where echo signals take some fifty seconds to return [1, 4, 12]. The downside of these sonars is the substantial error in target distance measurements. Theoretical analyses, simulation and experimental studies have shown that the errors are frequently so significant that they cannot be accepted by sonar users [5, 8, 9, 10, 11]. This led to the decision to develop a system designed to keep the target distance error significantly reduced. In general, the concept of the system is to use double modulation of sounding signals, and specifically hyperbolic frequency modulation (HFM) and code modulation via pseudo-random maximum length sequence (MLS) [2, 3, 5, 7, 9]. While the results of simulation tests presented in the publications confirm that the concept is generally right, they also point out that some of the sonar parameters are not as good as those of the CW FM sonar without code modulation. A general conclusion was formulated that acceptable sonar parameters can be achieved by selecting modulation parameters of sounding signals.

2. Principle of operation of the CW FM sonar with code modulation

The sonar's transmitter emits a periodical signal with period T, being a sequence of two types of wideband pulses with hyperbolic frequency modulation (HFM), different bands and duration T_i. The sequence corresponds to MLS of order N with $M = 2^N$-1 number of elements, thus $T_i \leq T/M$. The positive and negative elements of MLS are represented by HFM signals with non-overlapping frequency bands of width B_1 and an identical or opposite direction of frequency change over time. HFM signals whose frequency increases in time are described with the formula:

$$s^+(t) = s_o \sin[-2\pi \frac{T_i f_l^+ f_h^+}{B_1} ln\left(1 - B_1 \frac{t}{T_i f_h^+}\right)] \qquad t \in (0, T_i) \qquad (1)$$

while signals whose frequency decreases in time have this formula:

$$s^-(t) = s_o \sin[2\pi \frac{T_i f_l^- f_h^-}{B_1} ln\left(1 + B_1 \frac{t}{T_i f_l^-}\right)] \qquad t \in (0, T_i) \qquad (2)$$

where f_l^+, f_l^- are the lower and f_h^+, f_h^- are the upper spectral frequencies (different for positive and negative elements of the MLS sequence), and $B_1 = f_h^+ - f_l^+ = f_h^- - f_l^-$ is the spectral width (identical for positive and negative elements of the MLS sequence).

Fig. 1 shows one period of MLS sequence while Fig. 2 shows its corresponding period of a model low-band sequence. The time duration of rectangular pulses is T_p.

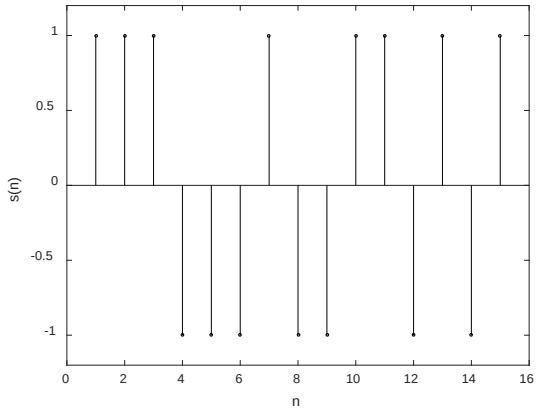

Fig. 1. A single period of MLS sequence (M = 15).

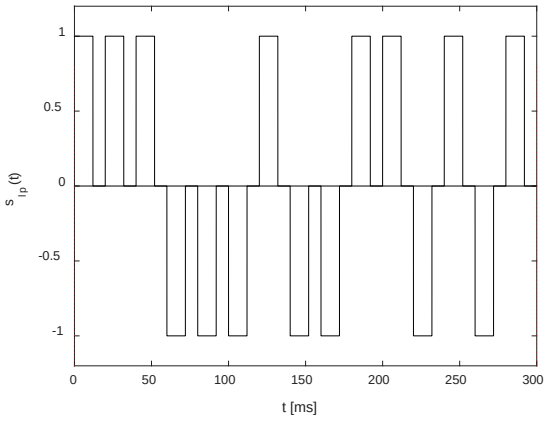

Fig. 2. A single period of low-band sequence (M=15, T_i = 20 ms, T_p = 12 ms).

Echo signal is processed in the sonar's receiver. Fig. 3 shows its functional diagram. Echo signal $x(t)$ is converted into a complex discrete signal $x(n)$ as a result of quadrature sampling or Hilbert transformation. The signal is then passed on to the inputs of two correlators, which calculate its correlation functions with signals, written in continuous form in formulas (1) or (2). The correlators perform matched filtration for signals which represent positive and negative elements of the MLS sequence. Signals from correlators' outputs are subtracted and the result is a bipolar sequence of correlation peaks. Fig. 4 shows a possible delayed sequence of peaks. The calculations were made for the following signal parameters: boundaries of the lower frequency band 9.0 kHz and 9.8 kHz, boundaries of the upper band 10.2 kHz and 11.0 kHz, frequency in both bands increases in time and M=15, T_i = 20 ms, T_p=12 ms, v = 0 and time delay t_0 = 40 ms.

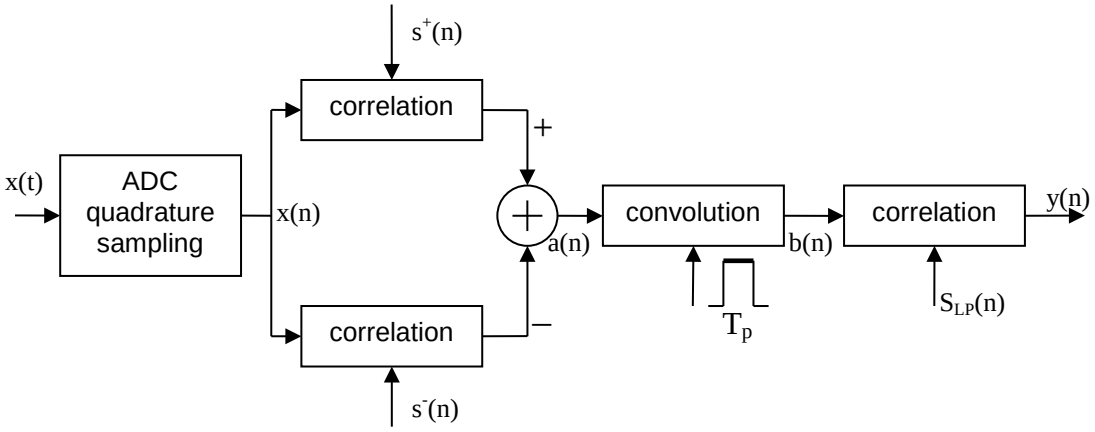

Fig. 3. Functional diagram of the receiver.

The sequence shown in Fig. 4 is convoluted with a rectangular pulse whose duration is T_p; as a result we obtain a low-band MLS sequence as shown in Fig. 5.

The objective of the final operation is to calculate the sequence's correlation to the model low-band MLS sequence, shown in Fig. 2. The correlation function is determined as shown in Fig. 6. It is an output signal to be detected in the sonar's receiver.

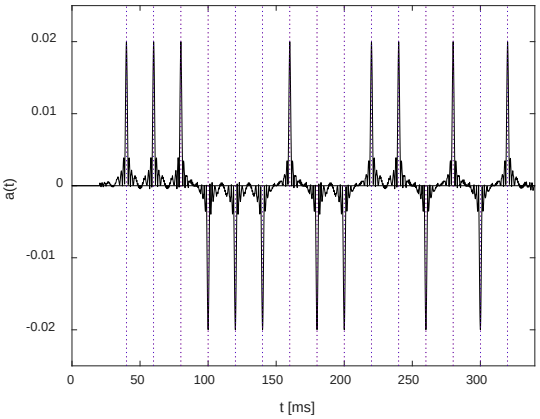

Fig. 4. Echo signal after correlation with elementary HFM signals and subtraction.

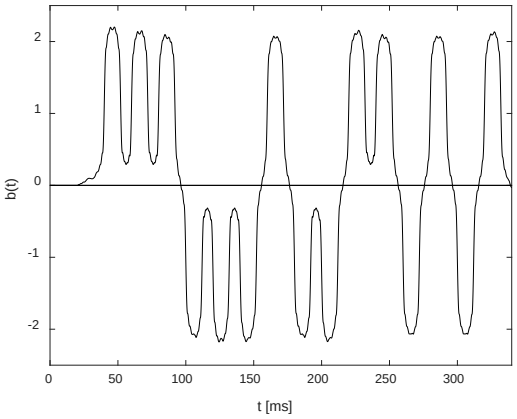

Fig. 5. Result of signal convolution with rectangular pulse.

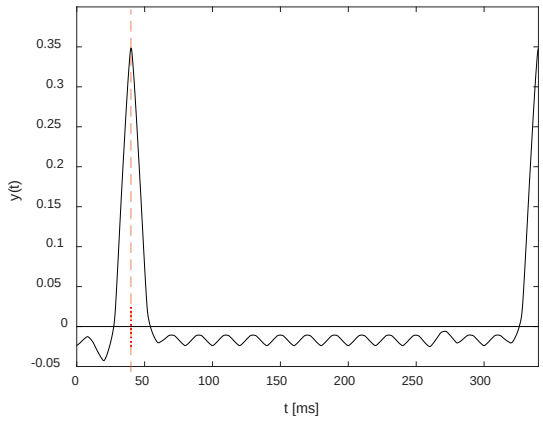

Fig. 6. Echo signal after correlation with model low-band MLS sequence.

The system's operating principle as discussed above reflects an ideal situation: the target is not moving relative to the sonar and the echo signal is an identical, shifted in time copy of the sounding signal with no noise. Further in the paper we will look at target distance errors, and how they change as we successively remove the above simplifications.

3. Target distance measurement error

The main reason why CW FM sonars produce wrong target distance measurements is the Doppler effect, the outcome of the sonar and target moving over time. It causes the echo signal to compress or expand making it not fully correlated to the transmitted signal. Incomplete correlation has a number of effects with target distance errors as the worst ones [5, 8, 9, 10]. Papers [2, 3, 5, 7, 9] have demonstrated that it is possible to reduce the errors if we use the sonar described above. How strong the reduction in error will be depends on practically all the signal parameters and receiver parameters.

How big the target distance error is depends primarily on two effects, namely the shift of the maximum of the HFM signal correlation and the shift of the maximum of the low-band MLS signal correlation function. Both shifts are the result of time compression which is described with compression coefficient *d*:

$$d = 1 + 2\frac{v}{c} \tag{3}$$

where *v* is how quickly the target moves towards the transmitter and *c* is the velocity of acoustic wave propagation in water. Time *t* after compression is *t/d*.

This is illustrated in Fig. 7 and Fig. 8 which show signals *a*(*t*) whose maxima have been shifted as a consequence of the Doppler effect. The blue broken lines show the positions of the maxima in the absence of the Doppler effect. The shift is [2]:

$$dt \cong 2T_p \frac{v}{c}\frac{f_m}{B_1} \tag{4}$$

where f_m is the middle frequency of the signal band. Where lower and upper bands stay close enough, the shift for both signals can be assumed to be the same.

The red broken line marks moments of time during which the receiver receives the frontal slopes of rectangular pulses. They are shifted relative to the blue lines as the target moves closer to or further away from the sonar. The position of these lines determines the low-band MLS after time compression.

In Fig. 7 the target is moving closer to the sonar and in Fig. 8 it is moving away. The frequency in left hand side figures is increasing in both bands. It increases in the right hand side lower figure and decreases in the upper one. As you can see, in the first case the shifts of positive and negative peaks are identical, but they are opposite in the second case. This is the outcome of formulas (1) and (2) which were found to be correct in an experiment [8]. These properties occur when the target is nearing the sonar (Fig. 7) and when it is moving away from it (Fig. 8). When the sign of target speed *v* changes, so does the time shift direction of correlation peaks sequence *a(t)*. The sequence's time is either compressed or expanded. Absolute values of the shifts are identical.

The signals *a*(*t*) exemplified above are convoluted with rectangular pulse of duration T_p. Fig. 9 shows how this operation affects signals depicted in Fig. 7. The charts are complemented with low-band sequences $s_{lp}(t)$ (red line) whose correlation function with signal *b*(*t*) is the output signal *y*(*t*). Fig. 10 shows the signal for the cases illustrated in Fig.8.

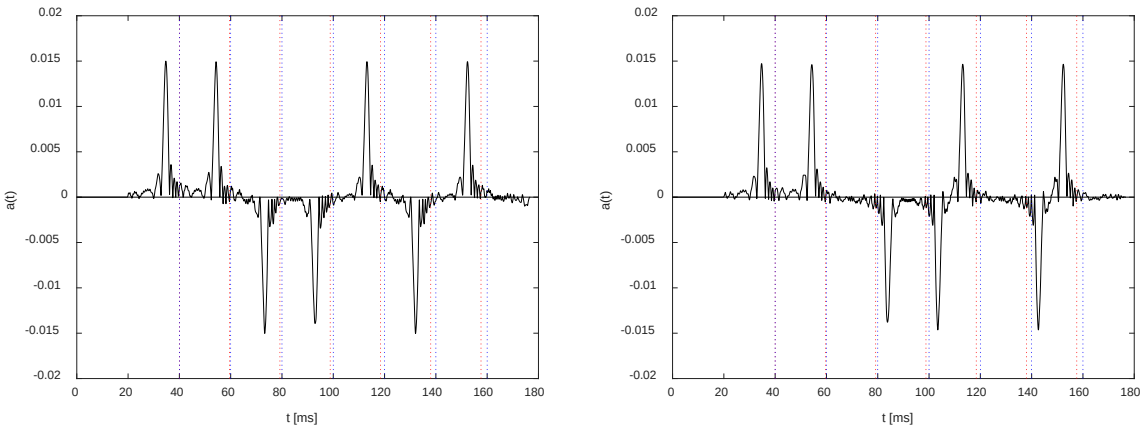

Fig.7. Time shifted *a(t)* sequence, the left hand side figure – the frequency in both bands is increasing, the right hand side – the frequency in the lower band is increasing and decreasing in the upper band (N = 3, lower band 9.0 - 9.8 kHz, upper band 10.2 - 11.0 kHz, T_i = 20 ms, v = 15 m/s).

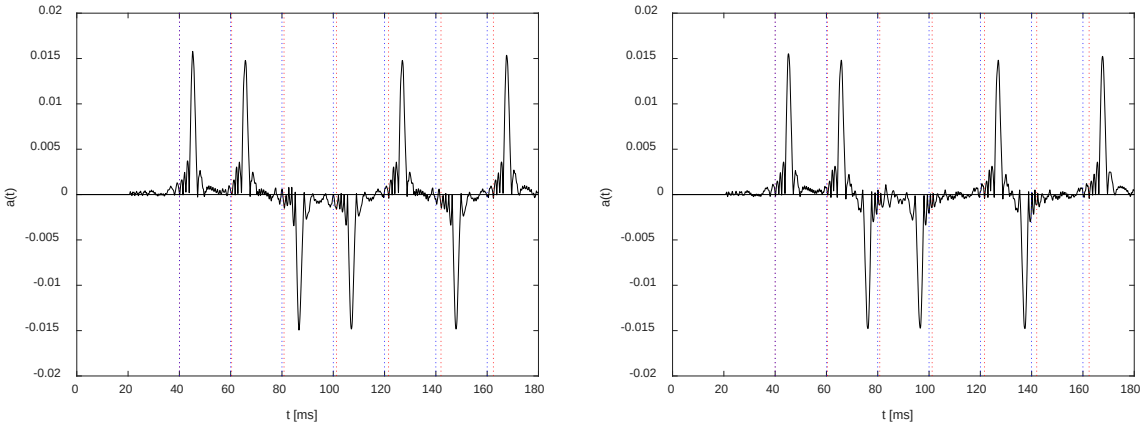

Fig.8. Time shifted *a(t)* sequence, the left hand side figure - the frequency in both bands is increasing, the right hand side – the frequency in the lower band is increasing and decreasing in the upper band (N = 3, lower band 9.0 - 9.8 kHz, upper band 10.2 - 11.0 kHz, T_i = 20 ms, v = - 15 m/s).

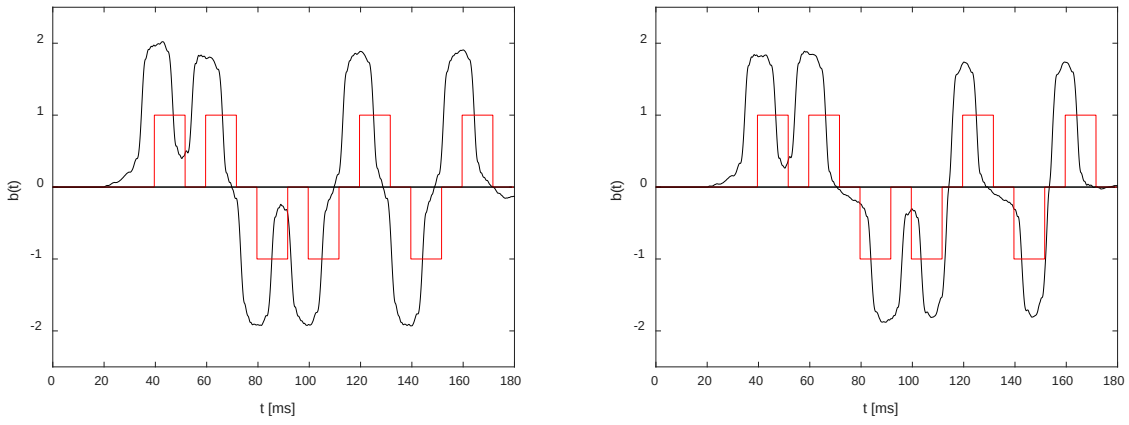

Fig.9. The result of convolution of time shifted *a(t)* sequence with rectangular pulse, left hand side figure – the frequency in both bands is increasing, right hand side figure– the frequency in the lower band is increasing and decreasing in the upper band (N = 3, lower band 9.0 - 9.8 kHz, upper band 10.2 - 11.0 kHz, T_i = 20 ms, T_p =12 ms, v = 15 m/s).

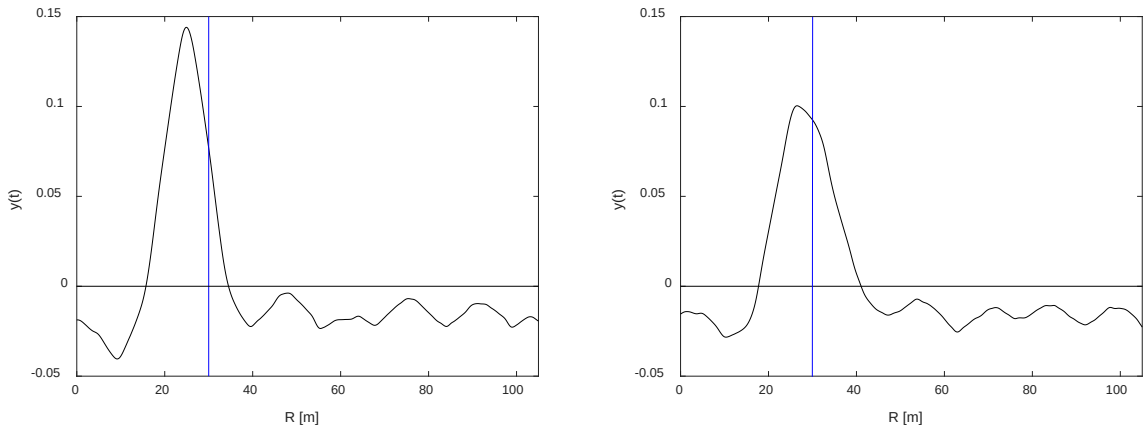

Fig.10. Output signal, left hand side figure – the frequency in both bands is increasing, the right hand side figure – the frequency in the lower band is increasing and decreasing in the upper band (N = 3, lower band 9.0 - 9.8 kHz, upper band 10.2 - 11.0 kHz, T_i = 20 ms, T_p = 12 ms, v = 15 m/s).

When the direction of frequency change is different for positive and negative pulses, the effects are as shown in Fig. 8. When the directions are the same, positive and negative pulses are almost identical. Their shifts grow systematically relative to the model low-band sequence. This causes time compression of the sequence received. The resulting distance measurement error ΔR consists of error dR related to HFM modulation and error which is the result of time compression of the low-band sequence. In the case shown in left hand side figures, error ΔR = 5.1 m, error $dR = 0.5 \cdot c\delta t$ = 3.8 m, and the compression-related error is 1.3 m. As you can see, in this example the target distance error is the sum of the discussed errors.

When frequency changes run in different directions (right hand side figures), there is a partial compensation of errors related to HFM signals and time compression of the low-band sequence. The compensation occurs for negative pulses. While it helps to reduce target distance error, now at ΔR = 3.5 m and close to error dR, it also reduces signal maximum value with a slight deterioration of resolution from 7.2 m to 10.1 m.

For fixed values T_i and T_p target distance measurement error ΔR increases as target speed v and sequence order N increase, as shown in Fig. 11 (parameters as in Fig. 10). For low orders N (3 to 5) the error increases linearly in the entire range of target speeds under consideration. For the majority of higher MLS sequence orders, the linear relation occurs for target speeds. For higher speeds the error increases faster. For all orders N and all speeds v, the target distance error is lower when HFM signal frequency changes run in opposite directions.

Despite a clear increase in target distance error, it is still lower than the error from comparable CW FM sonar without code modulation. This is illustrated in Fig. 12 which shows the errors generated by comparable sonar with the same middle frequency f_0, spectrum width B covering both frequency bands of HFM signals and duration equal to MT_i, and so the range is the same. The charts were made using formula [8]:

$$\Delta R \cong vMT_i \left(\frac{f_0}{B} + \frac{1}{2}\right) \qquad (5)$$

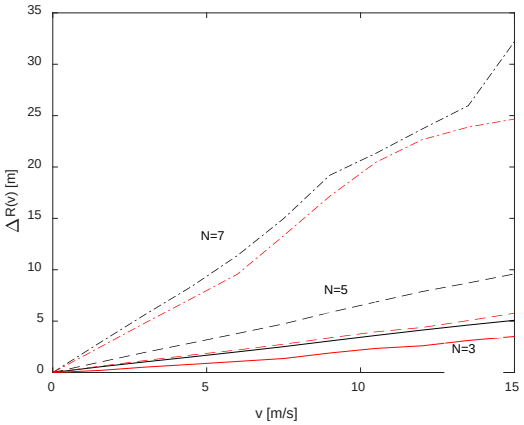

Fig.11. Distance measurement error in CW FM sonar with code modulation (black line – direction of frequency change in both bands the same, red line – opposite).

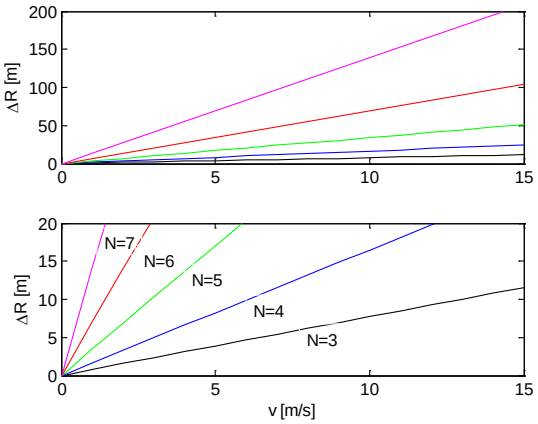

Fig.12. Distance measurement error in comparable CW FM sonar without code modulation (lower chart – zoom of the error range 0-20m).

The inclination of the straight line $a = \Delta R/v$ for orders of sequences $N = 3$, for a sonar with code modulation is $a = 0.16$, and for the comparable CW FM sonar $a = 0.77$. The differences in inclination are bigger for higher orders N. As an example, for $N = 5$, the inclination for a coded modulation sonar is $a = 0.36$ and $a = 3.41$ for a comparable CW FM sonar.

The Doppler effect deteriorates the resolution of distance measurement δR. Fig. 14 shows the changes in resolution corresponding to target distance errors from Fig. 11.

As sequence order and speed increase, a negative effect is produced, i.e. growth of side lobes, as shown in Fig. 13. As a consequence, detection performance suffers when a bigger number of targets is involved. The level of side lobes is shown in Fig. 15. It is defined as $L=20\log(y_{max}/y_{SLmax})$, where y_{SLmax} is the maximum of side lobes absolute value.

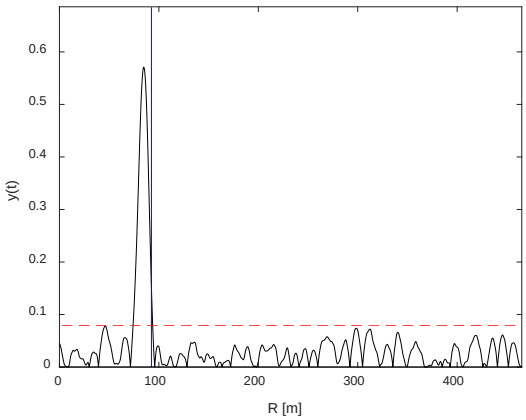

Fig. 13. Side lobes of output signal. ($N = 5$, T_i =20 ms T_p =12 v = 12 m/s)

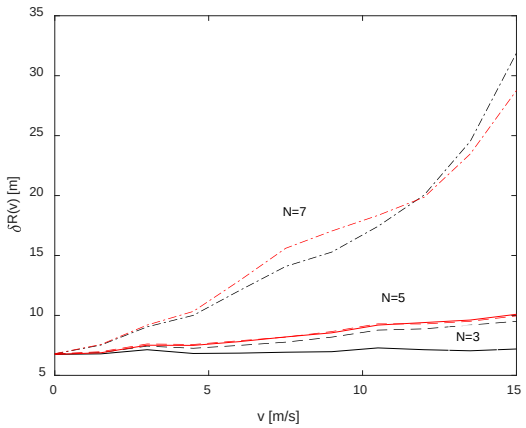

Fig. 14. Range resolution.

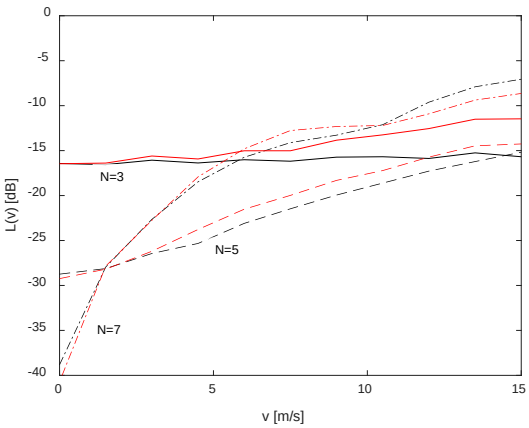

Fig. 15. Level of side lobes

As in Fig. 11, the black line in the figures above represents identical directions of frequency change in both bands while the red line shows opposite directions. For fixed values T_i and T_p, resolution and the level of side lobes both depend on the direction of frequency change of HFM signals. As you can see, having the same direction of frequency change is slightly better for distance resolution. For speed $v = 0$ resolution $\delta R = 6.8$ m. An analogous situation exists for the level of the side lobes.

Let us now consider the effect of pulse duration T_p for a fixed value of time T_i. In Fig. 16 and Fig. 17 this time is equal T_i=20 ms and the order of MLS sequence N=5.

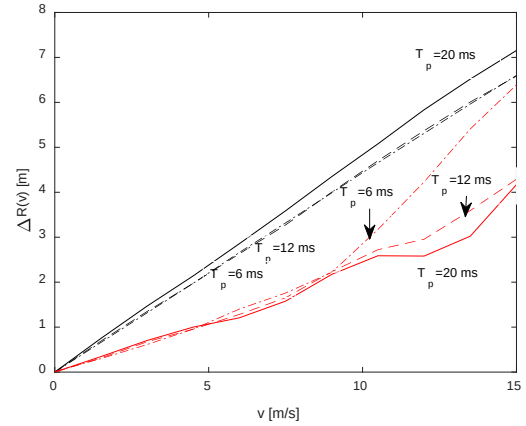

Fig. 16. Relation between distance error and pulse duration T_p (black line - the same direction of frequency change, red line - opposite direction).

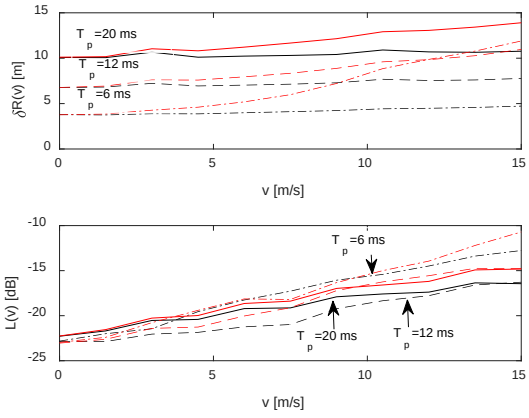

Fig. 17. Resolution and level of side lobes (denotation as in Fig.16).

Fig. 16 shows that the influence of time T_p on distance measuring error is negligible. However, it is preferable to use the opposite direction of frequency change of HFM. The shortening of the T_p time causes an improvement in the resolution δR, while excessive shortening of this time has a negative effect on the side lobes level.

The basic parameter of sonar design is its range R_{max}. Its nominal value is: $R_{max} = 0.5 \cdot c \cdot M \cdot T_i$. To achieve this, we can select different orders N of MLS sequences and different durations T_i. Depending on how these parameters are matched, the result will determine target distance error, resolution and side lobe level. This is illustrated in the figures below under the assumption that $R_{max} = 0.5 \cdot c \cdot T_i \cdot (2^N\text{-}1)$ [m], $T_i = 10 \cdot 2^{7-N}$ [ms], T_p=12 [ms]. Range $R_{max} \approx 950$ m. The calculations were made for a sonar watching slow moving targets, such as underwater vehicles (v=3 m/s) and vessels going at higher speeds such as submarines (v = 12 m/s).

The errors in target distance measurements are shown in Fig. 18. Fig. 19 presents the resolution and level of side lobes.

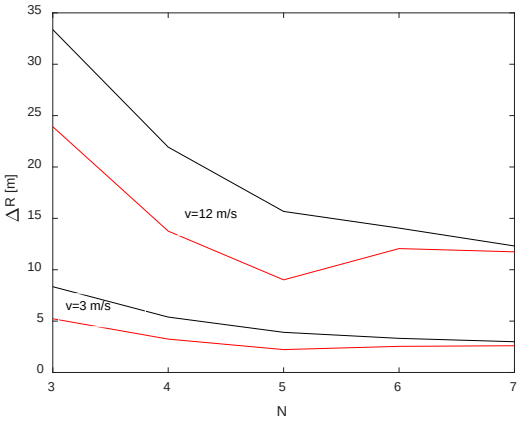

Fig. 18. Target distance error (directions of frequency change: black lines - the same, red lines - opposite).

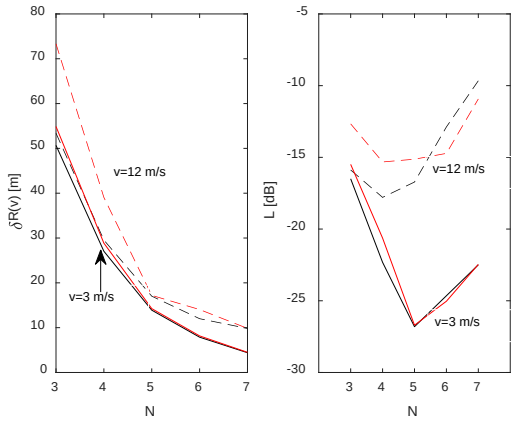

Fig. 19. Resolution and level of side lobes (marked as in Fig. 18).

In the example above the advantageous selection of MLS order is N=5. It ensures that target distance error is low, resolution is good and side lobe level is acceptable.

4. Conclusions

- A fundamental flaw of the classic CW FM sonar, the error in target distance measurements can now be eliminated entirely thanks to the proposed concept of silent sonar.
- To achieve desirable sonar parameters, we can select different orders N of MLS sequences and different durations T_i of elementary HFM signals. Depending on how these parameters are matched, the result will determine target distance error, resolution and side lobe level.
- To verify the simulation results in practice authors are going to build a model sonar based on the proposed design and test it on a measuring area.
- Unfortunately, the presented concept comes with certain deficiencies such as a deteriorated distance resolution and reduced echo signal dynamics. This affects detection conditions especially when more targets are involved.
- To minimize these negative features of CW FM sonar with MLS sequence code modulation, we are working intensively to improve its performance by using other types of pseudo-random sequences.

References

[1] H. DeFerrari, J. Wylie, Ideal signals and processing for continuous active sonar, Acoustical Society of America, Proceedings of Meetings on Acoustics (ICA 2013 Montreal Canada), Vol. 19, 055058, 2013.

[2] A. Jedel, J. Marszal, R. Salamon, Property analysis of the continuous wave sonar with pseudo random code modulation, [in Polish], in Progress of Acoustics, editor M. Meissner, Polish Acoustical Society, Warsaw Division, 485 – 498, 2016.

[3] A. Jedel, J. Marszal, R. Salamon, Continuous wave sonar with hyperbolic frequency modulation keyed by pseudo-random sequence, Hydroacoustics Vol. 19, 185-196, 2016.

[4] S. J. Lourey, Frequency Hopping Waveforms for Continuous Active Sonar, Proceedings of 2015 IEEE International Conference on Acoustics, Speech, and Signal Processing, 1832 – 1835, Brisbane 2015.

[5] J. Marszal, R. Salamon, A. Jedel, Silent Sonar – State of the Art and Perspectives [in Polish], in Progress of Acoustics, editor K. J. Opieliński, Polish Acoustical Society, Wroclaw Division, 31-48, 2015.

[6] J. Marszal, R. Salamon, Detection Range of Intercept Sonar for CWFM Signals, Archives of Acoustics, Vol. 39, No 2, 215-230, 2014.

[7] J. Marszal, R. Salamon, A. Jedel, Sounding Signal, Emitted Especially by a Silent Sonar, and Demodulation Method for a Sounding Signal, Emitted Especially by a Silent Sonar [in Polish], Patent Pending No. P.407692, 2014.

[8] J. Marszal, Experimental Investigation of Silent Sonar, Archives of Acoustics, Vol. 39, No 1, 103-115, 2014.

[9] J. Marszal, R. Salamon, Silent Sonar for Maritime Security Applications, Acoustical Society of America, Proceedings of Meetings on Acoustics (ECUA 2012 Edinburgh UK), Vol. 17, 070082, 2013.

[10] J. Marszal, R. Salamon, Distance Measurement Errors in Silent FM-CW Sonar with Matched Filtering, Metrology and Measurement Systems, Vol. XIX, No. 2, 321-332, 2012.

[11] J. Marszal, R. Salamon, K. Zachariasz, A. Schmidt, Doppler Effect in the CW FM Sonar, Hydroacoustics, Vol. 14, 157-164, 2011.

[12] R. van Vossen, S. P. Beerens, E. vander Spek, Anti-Submarine Warfare with Continuously Active Sonar, Sea Technology, Vol. 52**,** 11, 33-35, 2011.